PAPER • OPEN ACCESS

Interacting particles in an activity landscape

To cite this article: Adam Wysocki *et al* 2022 *New J. Phys.* **24** 093013

New Journal of Physics
The open access journal at the forefront of physics

Deutsche Physikalische Gesellschaft DPG
IOP Institute of Physics

Published in partnership with: Deutsche Physikalische Gesellschaft and the Institute of Physics

OPEN ACCESS

RECEIVED
2 April 2022

REVISED
5 August 2022

ACCEPTED FOR PUBLICATION
1 September 2022

PUBLISHED
15 September 2022

PAPER

Interacting particles in an activity landscape

Adam Wysocki[1,*], Anil K Dasanna[1,2] and Heiko Rieger[1,2]

[1] Department of Theoretical Physics and Center for Biophysics, Saarland University, Saarbrücken, Germany
[2] INM–Leibniz Institute for New Materials, Campus D2 2, 66123 Saarbrücken, Germany
[*] Author to whom any correspondence should be addressed.

E-mail: a.wysocki@lusi.uni-sb.de, anilkumar.dasanna@uni-saarland.de and heiko.rieger@uni-saarland.de

Keywords: active matter, phase separation, activity landscapes

Abstract

We study interacting active Brownian particles (ABPs) with a space-dependent swim velocity via simulation and theory. We find that, although an equation of state exists, a mechanical equilibrium does not apply to ABPs in activity landscapes. The pressure imbalance originates in the flux of polar order and the gradient of swim velocity across the interface between regions of different activity. An active–passive patch system is mainly controlled by the smallest global density for which the passive patch can be close packed. Below this density a critical point does not exist and the system splits continuously into a dense passive and a dilute active phase with increasing activity. Above this density and for sufficiently high activity the active phase may start to phase separate into a gas and a liquid phase caused by the same mechanism as motility-induced phase separation of ABPs with a homogeneous swim velocity.

1. Introduction

Active particles, like motile microorganisms, live in a complex environment and are affected by various external fields like gravity, fluid flows or walls [1]. Mostly it is assumed that their intrinsic properties, like propulsion speed or tumbling rate, are constant in space [2]. This is generally not true because organisms often respond to a spatially varying stimulus such as light intensity or chemical concentration. For example, the bacteria *E. coli* are chemotactic: they sense concentration gradients and adjust their tumbling rate to swim up or down a chemical gradient. Others do not respond to gradients but react in a non-directional way to the local stimulus intensity, a behavior called kinesis. For instance, some cyanobacteria are photokinetic and their swim speed depends on the local light intensity [3]. In this context, it has been predicted theoretically that the local density of particles $\rho(\mathbf{r})$ performing a run-and-tumble motion is inversely proportional to their local propulsion speed $v(\mathbf{r})$ [4]. This fact was used to arrange millions of light-powered bacteria into a complex pattern, such as Leonardo da Vinci's *Mona Lisa*, via light fields [5, 6]. Optical fields can also be used to create activity landscapes for synthetic microswimmers, such as thermophoretic Janus particles [7]. An activity landscape can have a technological application, such as traps [8] or rectifiers [9], but it can also be used to study fundamental questions of active matter [10, 11]. One such question is whether there is a coexistence criterion for active matter. The introduction of an active component of pressure [12, 13], often called 'swim pressure', allowed to formulate a mechanical equilibrium condition of equal pressures in phase separating purely repulsive active Brownian particles (ABPs) with a homogeneous propulsion speed [14]. The separation into a dense and a dilute phase is triggered by a slowdown during collisions and is named motility-induced phase separation (MIPS) [15–17]. The behavior of ABPs in activity landscapes, like the aggregation of particles in slow regions, resembles in some sense MIPS, however, the differences and similarities are not well studied. Here we show that an activity pattern can still lead to pressure imbalance between regions of different activity even though an equation of state exists for ABPs [14]. We show that, if the global density is low enough that all particles can be packed in the passive region, a critical point does not exist for an active–passive patch system, which continuously splits into a dense passive and a dilute active phase with increasing activity [18, 19]. However, if the passive patch is close packed, in addition to the separation according to the activity regions, the active

phase may also start to phase separate into a gas and a liquid phase caused by the same mechanism as MIPS [15–17] and thus leading to three-phase coexistence (dense passive, dense active and dilute active phase). The particles in the low activity region exhibit all states of matter of a two dimensional system: a liquid, a hexatic phase and a crystal. The transition to a state with a high orientational order for a sufficiently dense and active system can be predicted theoretically.

2. Model

We consider N ABPs in 2D with a space-dependent propulsion velocity $v(\mathbf{r})$. The particles interact via a repulsive pair potential $V(r) = \frac{k}{2}(\sigma - r)^2$ if $r \leqslant \sigma$, i.e., the inter-particle distance r is smaller then the particle diameter σ, and $V(r) = 0$ otherwise [20]. The repulsion strength k is chosen such that the particle overlap is 0.01σ during a head on collision. The positions $\mathbf{r}_i = (x_i, y_i)$ and the orientations $\mathbf{e}_i = (\cos\theta_i,\ \sin\theta_i)$ evolve according to the overdamped Langevin equations:

$$\dot{\mathbf{r}}_i = v(\mathbf{r}_i)\mathbf{e}_i + \mu_\mathrm{t}\sum_{j\neq i}\mathbf{f}_{ij} + \sqrt{2D_\mathrm{t}}\,\boldsymbol{\eta}_i \tag{1}$$

$$\dot{\theta}_i = \sqrt{2D_\mathrm{r}}\,\xi_i, \tag{2}$$

where $1/\mu_\mathrm{t} = \gamma_\mathrm{t}$ is the translational friction coefficient, $\mathbf{f}_{ij} = \mathbf{f}(\mathbf{r}_i - \mathbf{r}_j) = -\nabla_{\mathbf{r}_i}V(|\mathbf{r}_i - \mathbf{r}_j|)$ is the force on ith particle due to jth particle, D_t and D_r are the translational and rotational diffusion constant and $\boldsymbol{\eta}_i$, ξ_i are zero-mean unit-variance Gaussian white noises. For a spherical Brownian particle it is $D_\mathrm{r} = 3D_\mathrm{t}/\sigma^2$. We use a simulation box of size $L_x/\sigma = 320$ and $L_y/\sigma = 40$ (if not stated otherwise) with periodic boundary conditions in both directions and consider mainly a step-like activity landscape

$$v(x) = v_a\,\Theta\big(\alpha L_x/2 - |x|\big), \tag{3}$$

where Θ denotes the unit step function and α controls the extent of the active region ($\alpha = 0.5$ means that a half of the box is active). A dimensionless measure of activity is the normalized persistence length $Pe = v_a/(\sigma D_\mathrm{r})$ sometimes also called Péclet number, however, other definitions are also possible [12, 21]. The global packing fraction is defined as $\phi_0 = \pi(\sigma/2)^2 N/(L_x L_y)$.

3. Theory

First we ask whether a mechanical equilibrium exists or in other words: are pressures equal in neighbouring regions of different mobility?

Starting from (1) and (2) one obtains the full Smoluchowski equation [14, 22–24]

$$\partial_t\psi = D_\mathrm{t}\nabla^2\psi + D_\mathrm{r}\partial_\theta^2\psi - \nabla\cdot\left[v(\mathbf{r})\mathbf{e}\psi + \int \mathrm{d}\mathbf{r}'\,\mu_\mathrm{t}\mathbf{f}(\mathbf{r}'-\mathbf{r})\left\langle\hat{\rho}(\mathbf{r}')\hat{\psi}(\mathbf{r},\theta)\right\rangle\right] \tag{4}$$

for the time evolution of the noise-averaged probability density $\psi(\mathbf{r},\theta) = \langle\hat{\psi}\rangle = \langle\sum_{i=1}^{N}\delta(\mathbf{r}-\mathbf{r}_i)\,\delta(\theta-\theta_i)\rangle$, where $\langle\cdots\rangle$ denotes noise averages and $\hat{\rho} = \int \mathrm{d}\theta\,\hat{\psi}$ the fluctuating particle density. In the following we assume that the system is in the steady state, $\partial_t\psi = 0$, and is only inhomogeneous along the x-direction. Integrating (4) over θ gives

$$0 = \partial_x J_\rho(x) \tag{5}$$

with the particle flux

$$J_\rho(x) = v(x)m(x) + I_1(x) - D_\mathrm{t}\partial_x\rho(x), \tag{6}$$

where $m = \int \mathrm{d}\theta\cos(\theta)\psi$ is the polarisation and $I_1 = \int \mathrm{d}\mathbf{r}'\,\mu_\mathrm{t}f_x(\mathbf{r}'-\mathbf{r})\langle\hat{\rho}(\mathbf{r}')\hat{\rho}(\mathbf{r})\rangle$ is a contribution due to the pair-potential. Similarly, multiplying (4) by $\cos(\theta)$ and integrating over θ gives

$$D_\mathrm{r}m(x) = -\partial_x J_m(x) \tag{7}$$

with the flux of polar order

$$J_m(x) = v(x)\left\{\frac{\rho(x)}{2} + Q(x)\right\} + I_2(x) - D_\mathrm{t}\partial_x m(x), \tag{8}$$

where $Q = \frac{1}{2}\int \mathrm{d}\theta\,\cos(2\theta)\psi$ encodes nematic order along x-direction and $I_2 = \int \mathrm{d}\mathbf{r}'\,\mu_\mathrm{t}f_x(\mathbf{r}'-\mathbf{r})$ $\langle\hat{\rho}(\mathbf{r}')\hat{m}(\mathbf{r})\rangle$ contains the effect of interactions. All setups considered here are flux-free steady states, i.e., $J_\rho(x) = 0$. Thus inserting (7) into the vanishing particle flux J_ρ in (6) yields

$$0 = -\frac{v}{D_\mathrm{r}}\partial_x J_m + I_1 - D_\mathrm{t}\partial_x \rho. \tag{9}$$

Let us next consider two neighbouring domains A and B (ordered from left to right) with constant activity v_A and v_B, respectively. Then multiplying (9) with $\gamma_\mathrm{t} = k_\mathrm{B}T/D_\mathrm{t}$, integrating from the bulk of region A to the bulk of region B and using integration by parts gives

$$\int_A^B \mathrm{d}x\,(k_\mathrm{B}T\partial_x\rho - \gamma_\mathrm{t}I_1) = -\left[\frac{\gamma_\mathrm{t}}{D_\mathrm{r}} v J_m\right]_A^B + \frac{\gamma_\mathrm{t}}{D_\mathrm{r}}\int_A^B \mathrm{d}x\, J_m \partial_x v. \tag{10}$$

We define the ideal passive pressure as $p_\mathrm{id} = \rho k_\mathrm{B}T$, the interaction or 'direct' pressure as $\partial_x p_\mathrm{D} = -\gamma_\mathrm{t} I_1$ [22, 25] and the 'swim' pressure as $p_\mathrm{S} = \gamma_\mathrm{t} v^2\rho/2D_\mathrm{r} + \gamma_\mathrm{t} v I_2/D_\mathrm{r}$ [12, 22, 26]. For a homogeneous bulk phase in region A and B we can set $Q = m = 0$ and obtain finally

$$\left[p_\mathrm{id}(x) + p_\mathrm{D}(x) + p_\mathrm{S}(x)\right]_A^B = \frac{\gamma_\mathrm{t}}{D_\mathrm{r}}\int_A^B \mathrm{d}x\, J_m(x)\partial_x v(x), \tag{11}$$

which is the main result of our study.

Especially, for an activity step, where an ABP swims with v_A for $x < x_\mathrm{if}$ and abruptly propels with v_B when crossing the interface at $x = x_\mathrm{if}$, we get $\partial_x v = (v_B - v_A)\delta(x - x_\mathrm{if})$ and

$$\left[p_\mathrm{id}(x) + p_\mathrm{D}(x) + p_\mathrm{S}(x)\right]_A^B = \frac{\gamma_\mathrm{t}}{D_\mathrm{r}} J_m(x_{if})(v_B - v_A). \tag{12}$$

What does this mean? It means that the bulk pressures in both activity regions are not equal and that the pressure difference is governed by the activity profile $v(x_\mathrm{if})$ and the flux of polar order $J_m(x_\mathrm{if})$ at the interface between this regions. Thus an inhomogeneous activity pattern can still lead to unequal pressures in both phases even though an equation of state exists for ABPs [14]. The concept of pressure in active systems requires a comment here. One can show that if the entire system is confined by walls the normal force applied to the wall per unit area (wall pressure) equals the pressure far away from the wall (bulk pressure) independent of the shape of the wall potential. This implies that the pressure is a state function for ABPs and that the pressure is equal in coexisting phases in case of phase separation [14, 22]. A similar expression as (11) have been obtained for underdamped quorum-sensing active particles undergoing MIPS [27], which lack an equation of state for the pressure even for spatially uniform activity [14].

Next, we examine the case of non-interacting ABP's, which can be solved exactly in all details [10, 28]. In particular, let us consider a setup where particles are inactive ($v_p = 0$) for $x < x_\mathrm{if} = 0$ and are active ($v_a > 0$) for $x > 0$. We non-dimensionalize (12) using $\pi\sigma^2/(4k_\mathrm{B}T)$. The left-hand side of (12) reads as

$$\frac{\pi\sigma^2}{4k_\mathrm{B}T}\left[p_\mathrm{id}(x) + p_\mathrm{S}(x)\right]_p^a = \phi_a\left(1 + \frac{v_a^2}{2D_\mathrm{t}D_\mathrm{r}}\right) - \phi_p = \left(\frac{\lambda_p}{\lambda_a} - 1\right)\phi_p \tag{13}$$

using the bulk density ratio $\lambda_a/\lambda_p = \rho_a/\rho_p$ [10, 18, 19, 28, 29], where ρ_α is the bulk density in region $\alpha = \{a, p\}$, respectively, $\lambda_\alpha = \left(D_\mathrm{r}/D_\mathrm{t} + v_\alpha^2/2D_\mathrm{t}^2\right)^{-1/2}$ denotes the polarisation decay length and $\phi_\alpha = \pi(\sigma/2)^2\rho_\alpha$ the packing fraction. In the following we use the polarisation profile obtained in [10, 28], which in the passive region ($x < 0$) takes the form $m(x) = m_\mathrm{max}\exp(x/\lambda_p)$ with $m_\mathrm{max} = -v_a\rho_p\lambda_a\lambda_p/2D_\mathrm{t}(\lambda_a + \lambda_p)$ for our particular setup. In order to calculate the right-hand side of equation (12) we use

$$J_m(0) = \int_{-\infty}^0 \mathrm{d}x\,\partial_x J_m(x) = -D_\mathrm{r}\int_{-\infty}^0 \mathrm{d}x\, m(x) = -D_\mathrm{r} m_\mathrm{max}\lambda_p, \tag{14}$$

where $J_m(-\infty) = 0$ because of $v(-\infty) = m(-\infty) = 0$, see (8) for the individual terms of J_m. In total we get for the right-hand side of (12)

$$\frac{\pi\sigma^2}{4k_\mathrm{B}T}\frac{\gamma_\mathrm{t}}{D_\mathrm{r}} J_m(0) v_a = \left(\frac{\lambda_p}{\lambda_a} - 1\right)\phi_p > 0, \tag{15}$$

which equals (13) and thus proves the validity of (12) for the ideal system. Due to $\lambda_p > \lambda_a$, the pressure in the active region is larger than the pressure in the passive region.

With (12) we want to estimate the packing fractions ϕ_a and ϕ_p of interacting particles in an active–passive patch system. An approximate equation of state for interacting ABP's in 2D [30] reads as

$$p_a(\rho_a, Pe) = p_{\mathrm{id}} + p_{\mathrm{D}} + p_{\mathrm{S}} = \rho_a k_{\mathrm{B}} T \left[1 + \frac{3}{2\pi} \frac{Pe\,\phi_a}{1 - \frac{\phi_a}{\phi_{\max}}} + \frac{3}{8} Pe^2 \left(1 - \frac{\phi_a}{\phi_{\max}} \right) \right], \tag{16}$$

where $\phi_{\max} = \pi/\sqrt{12}$ is the packing fraction of a close-packing of monodisperse disks. The 'swim' pressure vanishes while the interaction pressure diverges at $\phi_{\max}$. For passive hard disks we use [31]

$$p_p(\rho_p) = \rho_p k_{\mathrm{B}} T \left(1 - 2\phi_p + \frac{2\phi_{\max} - 1}{\phi_{\max}^2} \phi_p^2 \right)^{-1}, \tag{17}$$

which, however, does not capture the existence of a 'hexatic' phase at $\phi \in [0.7, 0.72]$, see [32]. We obtain one equation by inserting (16) and (17) into (12) using the interface contribution of non-interacting particles (15), however, with a density dependent activity $v(\phi) = v_a(1 - \phi/\phi_{\max})$. And we get another equation by assuming a rectangular density profile with constant values ϕ_a and ϕ_p such that $\phi_0 = \alpha\phi_a + (1 - \alpha)\phi_p$. The numerical solution of these two equations give the densities ϕ_a and ϕ_p for each Pe and ϕ_0. The approximation of the interface term works only up to a moderate ϕ_0 and the assumption of a constant density fails if the active phase gets inhomogeneous as in the case of MIPS.

4. Results

Figures 1(a) and (b) shows snapshots of a system with a step-like activity pattern with $\alpha = 0.5$, i.e., half of the box, namely $[-L_x/4, L_x/4]$, is active and passive otherwise. In figures 1(a), (c) and (e) the global packing fraction is $\phi_0 = 0.4 < (1 - \alpha)\phi_{\max} \approx 0.4534$ and the maximum possible packing fraction in the passive patch is below close-packing. Figure 1(a) demonstrates the general behavior of a system with a position dependent activity $v(\mathrm{r})$, namely, that particles tend to accumulate in the less mobile region or in other words, $\rho \propto 1/v$ [4, 33]. A strong positive polarization m (particles point toward the passive region) appears solely at the active–passive interface and is zero otherwise, see figure 1(c). The mechanism responsible for this polarization is similar to that of ABP's near walls [34, 35], only the particles that point toward the interface can also approach it and once they cross the interface they keep their orientation for a time scale $\tau_r = 1/D_{\mathrm{r}}$. In figure 1(e) we show the normal component of the local 'swim' $p_{\mathrm{S}}(x)$ [36] and interaction pressure tensor $p_{\mathrm{D}}(x)$ [37]. Surprisingly, the total pressure is not equal in both regions, even though an equation of state for ABPs exists [14], and is larger in the dilute active region, where the 'swim' pressure p_{S} is the dominant contribution. What balances this pressure gradient? One can take two points of view. If one argues that the 'true' pressure consists only of the ideal p_{id} and the 'direct' pressure p_{D} (neglecting the 'swim' pressure p_{S}) then the pressure gradient is balanced by the swim force density $\gamma_{\mathrm{t}} vm$ created by the polarization of the active particles [38] or in other words

$$\partial_x \left(p_{\mathrm{id}} + p_{\mathrm{D}} \right) = \gamma_{\mathrm{t}} v(x) m(x), \tag{18}$$

which follows from $J_\rho(x) = 0$ and is a local force density balance equation. For our case that means that the dense passive phase is held together by the rim of polarized particles in the active region. If one also considers p_{S} then the pressure gradient is balanced by the term on the right-hand side of (11) consisting of the flux of polar order J_m and the gradient in the activity $\partial_x v$.

Our particles are hard disks and can only be packed till $\phi_{\max}$. We expect two regimes based purely on packing properties in the passive region. In the following we refer to ϕ_a and ϕ_p as the average values of $\phi(x)$ over the active and the passive region, respectively. In the limit of high activity, $Pe \to \infty$, we expect

$$\phi_a = 0 \quad \text{and} \quad \phi_p = \frac{\phi_0}{1 - \alpha} \quad \text{for} \quad \phi_0 < (1 - \alpha)\phi_{\max}, \tag{19}$$

which is the regime discussed so far, and

$$\phi_a = \frac{\phi_0 - (1 - \alpha)\phi_{\max}}{\alpha} \quad \text{and} \quad \phi_p = \phi_{\max} \quad \text{for} \quad \phi_0 \geqslant (1 - \alpha)\phi_{\max}. \tag{20}$$

A system above overcrowding, $\phi_0 = 0.7 \geqslant (1 - \alpha)\phi_{\max} \approx 0.4534$, is shown in figures 1(b), (d) and (f). The passive patch is nearly close-packed and the active patch consists of a dilute and a dense phase, the latter localized near the passive one. We will discuss the link to MIPS of a purely active system below [20, 22, 30]. The polarized region is no longer located at the active–passive boundary but at the interface between the dilute and the dense active phase, see figure 1(d). The pressure is equal in both active phases, however, there is still a small but finite pressure jump across the active–passive boundary, see figure 1(f).

ABPs with a homogeneous propulsion speed separate only above a critical point $Pe_{\mathrm{cr}} \approx 13.3$, $\phi_{\mathrm{cr}} \approx 0.597$ into a dense and a dilute phase [21]. The densities of the coexisting phases are independent of

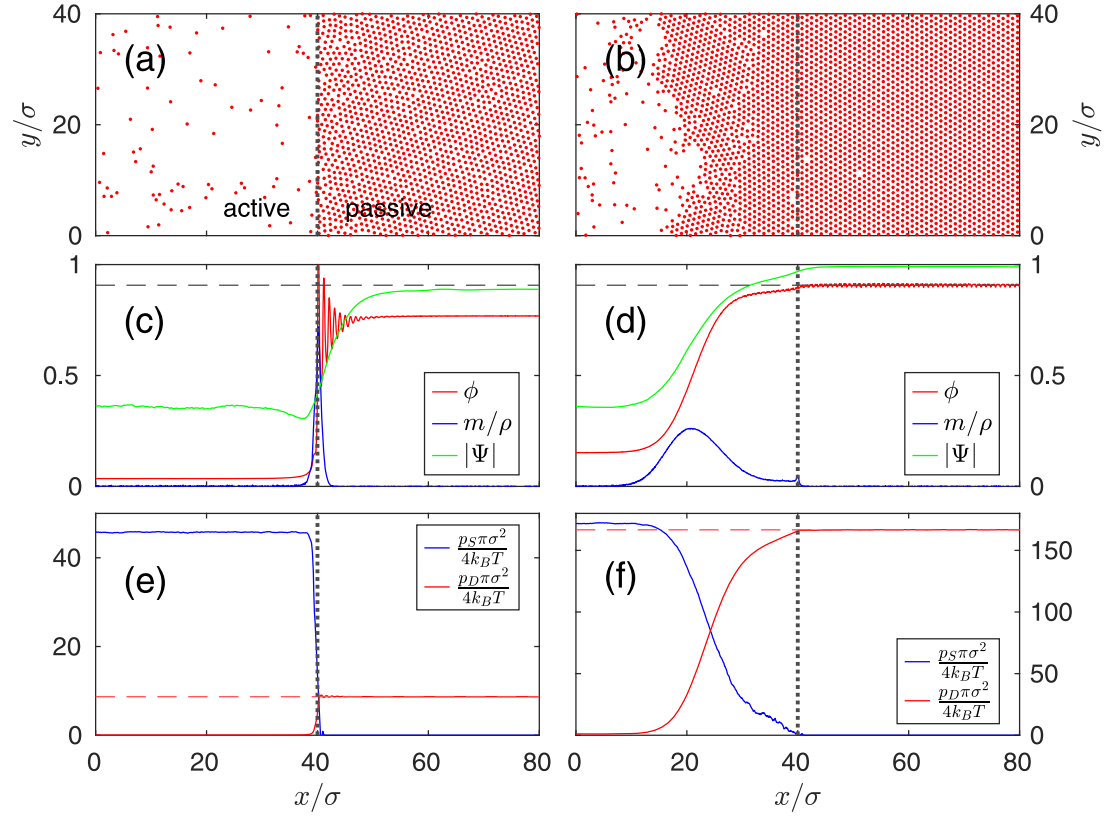

Figure 1. (a) and (b) Snapshots of ABPs in an active–passive patch system for two different global packing fractions $\phi_0 = 0.4$ (left column) and $\phi_0 = 0.7$ (right column) but for the same activity $Pe = 30$. (c) and (d) The corresponding profiles of the packing fraction $\phi(x) = \pi(\sigma/2)^2\rho(x)$ (red) and polarization $m(x)/\rho(x)$ (blue) and magnitude of the local bond-orientational order parameter $|\Psi|(x)$ (green). The horizontal dashed line indicates $\phi_{\max} = \pi/\sqrt{12}$. (e) and (f) The local 'swim' $p_S(x)$ (red) and 'direct' pressure profiles $p_D(x)$ (blue). The red horizontal dashed line illustrates the pressure difference between the active and the passive region. Only half of the simulation box is shown $[0, L_x/2]$ and the dotted vertical line at $x = L_x/4$ indicates the interface between the active (left) and the passive region (right), i.e., the fraction of the active region is $\alpha = 0.5$. Lengths are scaled by the particle diameter σ.

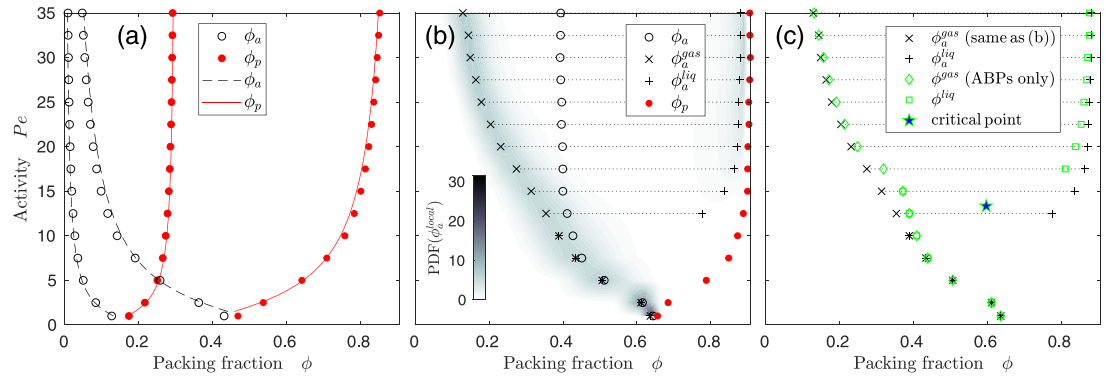

Figure 2. (a) The average values of $\phi(x)$ over the active and the passive region, ϕ_a and ϕ_p, respectively, as a function of the activity Pe for two different global packing fractions $\phi_0 = 0.15$ and $\phi_0 = 0.45$, below overcrowding, $\phi_0 < (1-\alpha)\phi_{\max} \approx 0.4534$ with $\alpha = 0.5$, obtained from simulations (circles and dots) and theory (dashed and solid lines). (b) Circles and dots indicate ϕ_a and ϕ_p versus Pe for $\phi_0 = 0.65 \geqslant (1-\alpha)\phi_{\max}$. The heat map represents the distribution of the local density in the active region ϕ_a^{local}. The maxima of this distribution, which represents the densities of coexisting phases in the active patch ϕ_a^{gas} and ϕ_a^{liq}, are marked by $\times$ and $+$, respectively. (c) Comparison between phase separation in the active patch (same symbols $\times$ and $+$ as in (b)) and MIPS in an equivalent purely active system (ϕ^{gas} and ϕ^{liq} are marked by $\diamond$ and $\square$). The purely active system is of the same size as the active patch, $[-\alpha L_x/2, \alpha L_x/2]$, and at the same average packing fraction ϕ_a. In addition, the critical point of ABPs is shown [21].

the global density ϕ_0 at fixed activity Pe. The situation is different for a system with a mobility pattern. In figure 2(a) the mean packing fractions in the active and the passive patch, ϕ_a and ϕ_p, as a function of Pe below overcrowding are show. No signs of a critical point are visible, i.e., the system splits continuously,

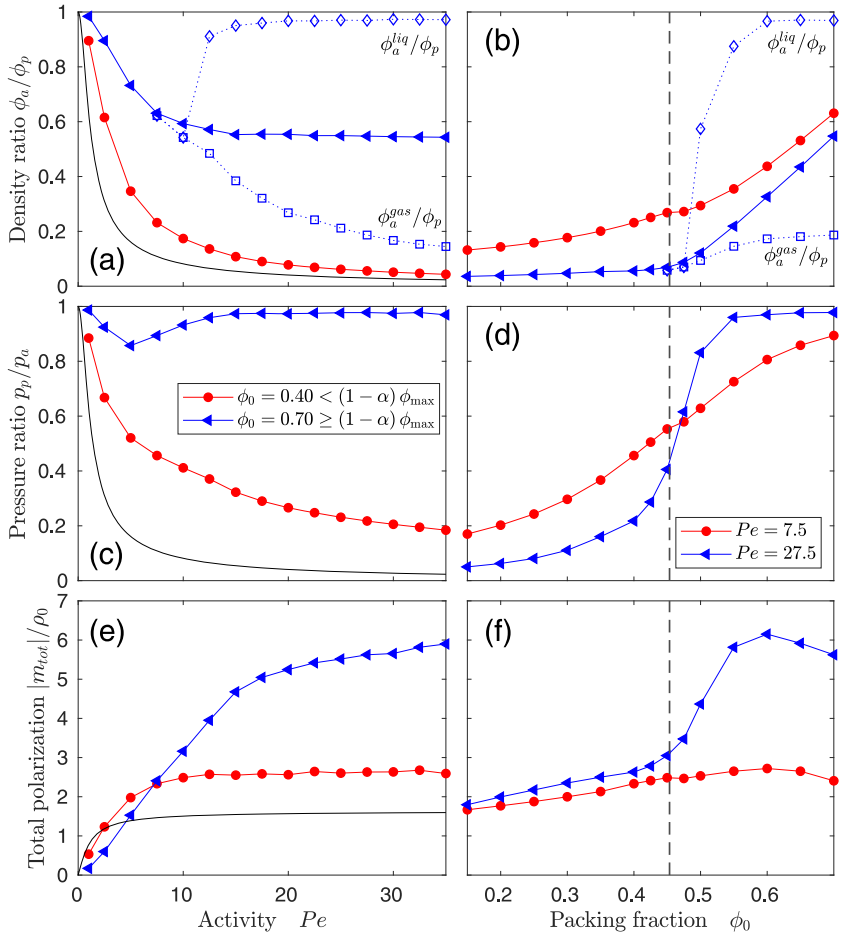

Figure 3. (a) and (b) Density ratio ϕ_a/ϕ_p, (c) and (d) pressure ratio p_p/p_a and (e) and (f) the total interface polarization $m_{\rm tot} = \int_a^p {\rm d}x\, m(x)$ for varying activities Pe and global packing fractions ϕ_0 are shown. In (a), (c) and (e) the solid black lines indicate the exact results for the non-interacting case. The densities ϕ_a and ϕ_p and pressures p_a and p_p are averages over the active and passive patch, respectively. If the phase in the active region becomes unstable it separates into a gas and a liquid phase with densities $\phi_a^{\rm gas}$ and $\phi_a^{\rm liq}$, respectively. The vertical dashed line in (b), (d) and (f) is drawn at $\phi_0 = (1-\alpha)\phi_{\max} \approx 0.4534$ with $\alpha = 0.5$ and indicates the global packing fractions ϕ_0 above which the passive patch is closely packed in the limit of $Pe \to \infty$.

starting at $Pe = 0$, into a dense passive and a dilute active phase with increasing Pe. In the limit $Pe \to \infty$ all particles occupy the passive patch, cf (19). Moreover, figure 2(a) demonstrates that the theory, based on (12), agree very well with the simulation results for densities below overcrowding. Above overcrowding, as was already visible in figure 1(b), the behaviour is more complex. Figure 2(b) shows in addition to ϕ_a and ϕ_p also the distribution of the local density in the active region $\phi_a^{\rm local}$ obtained from Gaussian coarse graining [39]. Just as below overcrowding, the system first splits continuously into a dense passive and a dilute active phase with increasing Pe. However, above some Pe the active phase becomes unstable and separates in to a gas and a liquid phase with densities $\phi_a^{\rm gas}$ and $\phi_a^{\rm liq}$, respectively. The active liquid phase is localized near the dense passive phase, see $\phi(x)$ in figure 1(d), and their densities are different ($\phi_a^{\rm liq} \neq \phi_p$). In order to check if this secondary instability appears as soon as $\phi_a(Pe)$ enters the coexistence region of ABPs [20, 22, 30] we have simulated a purely active system of the same size as the active patch and at the same mean packing fraction ϕ_a. In figure 2(c) we show the coexisting densities, $\phi_a^{\rm g}$ and $\phi_a^{\rm l}$, of a inhomogeneous and, $\phi^{\rm g}$ and ϕ^{ℓ}, of a corresponding homogeneous system. We see that the inhomogeneous system phase separates at lower Pe as compared to the homogeneous one. This difference is probably due to the presence of the dense passive phase, which acts as a wall and thus leads to an accumulation of active particles [34, 35]. We speculate that for an infinite system this effect should become negligible and the coexisting densities in the active patch should match the binodal of ABPs. Furthermore, the question arises whether the active phase can become unstable below overcrowding. Several papers [21, 22] indicate that the gas branch of two-dimensional ABPs does not terminate at zero density for large Pe, i.e., $\lim_{Pe\to\infty} \phi^{\rm g} > 0$. If this is true then it is not possible for $\phi_a(Pe)$ to enter the MIPS region for $\phi_0 < (1-\alpha)\phi_{\max}$ due to $\lim_{Pe\to\infty} \phi_a = 0$.

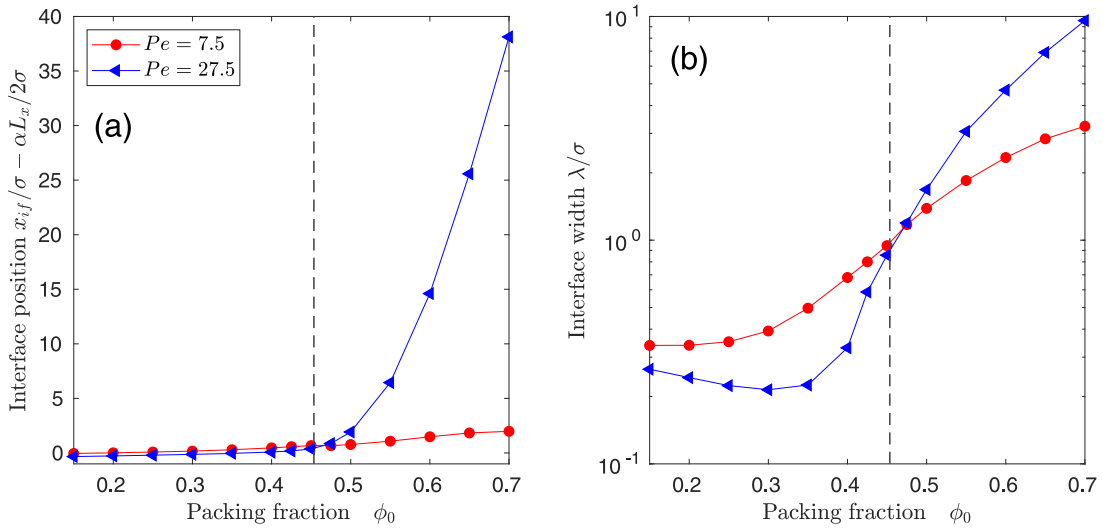

Figure 4. (a) Interface position x_{if} and (b) the interface width λ as function of the overall packing fraction ϕ_0 for two activities Pe. The vertical dashed line is drawn at $\phi_0 = (1-\alpha)\phi_{\mathrm{max}} \approx 0.4534$ with $\alpha = 0.5$, which marks the border of overcrowding in the limit of $Pe \to \infty$.

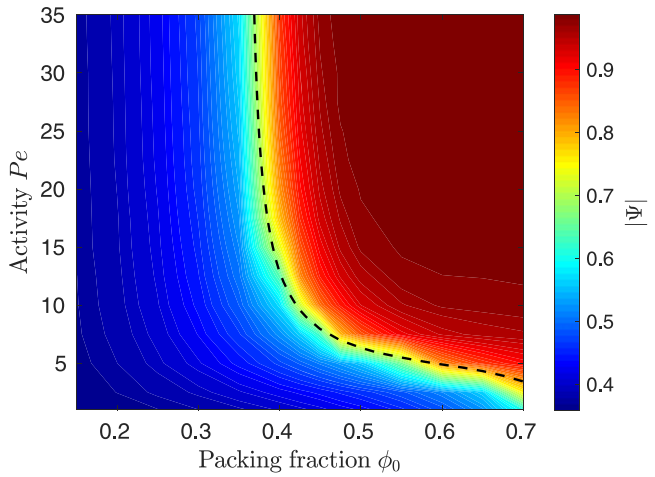

Figure 5. Average magnitude of the local bond-orientational order parameter $|\Psi|$ within the passive region as function of the global packing fraction ϕ_0 and activity Pe. For a perfect triangular lattice $|\Psi| = 1$. The isoline $\phi_p(\phi_0, Pe) = 0.716$ (black dashed line) indicates the transition to a pure hexatic phase [32] and is a numerical result of the theory based on (12).

Figure 3 indicates the interdependencies between the densities of the coexisting phases, the corresponding pressures and the total polarisation. Below overcrowding, the density and the pressure ratio decreases as in the ideal case, $\phi_a/\phi_p \propto p_p/p_a \propto 1/Pe$, see figures 3(a) and (c). However, above overcrowding, ϕ_a/ϕ_p saturates at a finite value with increasing Pe, see figure 3(a), or increases linearly with ϕ_0, see figure 3(b), which in both cases is in line with (20). In addition, only above overcrowding, ϕ_a/ϕ_p bifurcates above some Pe or ϕ_0 into a gas and a liquid branch due to phase separation in the active patch (cf discussion of figure 2), see figures 3(a) and (b), and the pressure in both regions is almost the same ($p_p/p_a \approx 1$), see figures 3(c) and (d). The total interface polarisation $m_{\mathrm{tot}} = \int_a^p \mathrm{d}x\, m(x)$, which is proportional to the difference of the bulk flux of polar order J_m in the active to the passive region [40], saturates with increasing Pe, see figure 3(e). Besides the trivial dependency $m_{\mathrm{tot}} \propto \phi_0$ there is a pronounced change in growth of m_{tot} as a function of ϕ_0 at $(1-\alpha)\phi_{\mathrm{max}}$ for large Pe, see figure 3(f). Once the passive patch is fully occupied active particles start to wet the dense passive phase, which means that the position of the interface between the dense and the dilute phase x_{if} does not coincide anymore with the active–passive boundary $\alpha L_x/2$, see figure 4(a). The interface start to fluctuate strongly and its width λ increases significantly once the phase separation sets in, see figure 4(b), resembling the behaviour of an interface during MIPS [41]. We obtained x_{if} and λ by fitting the density profile with a hyperbolic tangent.

As clearly visible in figure 1(a), the less active patch has a much higher particle density than the other. However, monodisperse disks can only be packed up to $\phi_{\max} = \pi/\sqrt{12}$ arranged in a hexagonal lattice [42] and thus a crystalline order in the less mobile region is expected for a sufficiently dense and active system. Hexagonal packing has a long-range orientational (sixfold) order, which can be measured using the local hexatic order parameter $\Psi(\mathbf{r}_j) = \sum_{k=1}^{N_j} \exp(\mathrm{i}6\theta_{jk})/N_j$, where θ_{jk} is the angle formed by the bond that connects the jth disk and its kth (out of N_j) nearest neighbor (found with a Voronoi tessellation algorithm) and the x axis [32]. For a perfect triangular lattice, all the angles $6\theta_{jk}$ are the same and $|\Psi(\mathbf{r}_j)| = 1$. Because of the polycrystalline character of the dense phase we use the average magnitude of the hexatic order parameter $|\Psi| = \sum_{i=1}^{N} |\Psi(\mathbf{r}_i)|/N$ in order to get a global information on the order [43], which however does not vanish in an isotropic fluid. In figure 5 the order parameter $|\Psi|$ within the passive patch as function of ϕ_0 and Pe is shown. $|\Psi|$ displays a sharp increase beyond the isoline $\phi_p(\phi_0, Pe) = 0.716$ (dashed line), which indicates the transition to a pure hexatic phase [32] and is a numerical result of the theory based on (12). The minimum global packing fraction necessary for a crystalline patch is $\phi_0 = (1 - \alpha)0.716$.

5. Summary

To summarize our main findings: we have theoretically justified the pressure imbalance in an activity landscape. The pressure difference originates in the flux of polar order and the gradient of swim velocity across the interface between regions of different activity. We found that although the density is lower in the more active area the corresponding pressure is higher. For systems below overcrowding, $\phi_0 < (1 - \alpha)\phi_{\max}$, the densities in the active and the passive patch can be predicted from the balance equation (11). Moreover, we have studied the effect of interactions on ABPs in activity landscapes. Excluded volume effect become significant above a global packing fraction $\phi_0 = (1 - \alpha)\phi_{\max}$, namely, when the passive patch is completely filled with particles in the limit $Pe \to \infty$. In that case the active phase can enter the binodal of ABPs (the coexistence region of a system with a homogeneous swim velocity) above some Pe and ϕ_0, with the result that the overall system consists of three phases: a dense passive, a dense active and a dilute active phase. The dense phase in the less-active region exhibits a crystalline order for a sufficiently dense and active system, and the transition line can also be predicted from the balance equation (11).

Acknowledgments

This work was financially supported by the German Research Foundation (DFG) within the Collaborative Research Center SFB 1027.

Data availability statement

The data that support the findings of this study are available upon reasonable request from the authors.

ORCID iDs

Anil K Dasanna https://orcid.org/0000-0001-5960-4579

References

[1] Bechinger C, Di Leonardo R, Löwen H, Reichhardt C, Volpe G and Volpe G 2016 Active particles in complex and crowded environments *Rev. Mod. Phys.* **88** 045006
[2] Shaebani M R, Wysocki A, Winkler R G, Gompper G and Rieger H 2020 Computational models for active matter *Nat. Rev. Phys.* **2** 181–99
[3] Wilde A and Mullineaux C W 2017 Light-controlled motility in prokaryotes and the problem of directional light perception *FEMS Microbiol. Rev.* **41** 900–22
[4] Schnitzer M J 1993 Theory of continuum random walks and application to chemotaxis *Phys. Rev.* E **48** 2553–68
[5] Frangipane G, Dell'Arciprete D, Petracchini S, Maggi C, Saglimbeni F, Bianchi S, Vizsnyiczai G, Bernardini M L and Di Leonardo R 2018 Dynamic density shaping of photokinetic *E. coli eLife* **7** e36608
[6] Arlt J, Martinez V A, Dawson A, Pilizota T and Poon W C K 2018 Painting with light-powered bacteria *Nat. Commun.* **9** 768
[7] Söker N A, Auschra S, Holubec V, Kroy K and Cichos F 2021 How activity landscapes polarize microswimmers without alignment forces *Phys. Rev. Lett.* **126** 228001
[8] Jahanshahi S, Lozano C, Liebchen B, Löwen H and Bechinger C 2020 Realization of a motility-trap for active particles *Commun. Phys.* **3** 127
[9] Stenhammar J, Wittkowski R, Marenduzzo D and Cates M E 2016 Light-induced self-assembly of active rectification devices *Sci. Adv.* **2** e1501850

[10] Auschra S, Holubec V, Söker N A, Cichos F and Kroy K 2021 Polarization-density patterns of active particles in motility gradients *Phys. Rev.* E **103** 062601
[11] Caprini L, Marini Bettolo Marconi U, Wittmann R and Löwen H 2022 Dynamics of active particles with space-dependent swim velocity *Soft Matter* **18** 1412–22
[12] Takatori S C, Yan W and Brady J F 2014 Swim pressure: stress generation in active matter *Phys. Rev. Lett.* **113** 028103
[13] Winkler R G, Wysocki A and Gompper G 2015 Virial pressure in systems of spherical active Brownian particles *Soft Matter* **11** 6680–91
[14] Solon A P, Fily Y, Baskaran A, Cates M E, Kafri Y, Kardar M and Tailleur J 2015 Pressure is not a state function for generic active fluids *Nat. Phys.* **11** 673–8
[15] Fily Y and Marchetti M C 2012 Athermal phase separation of self-propelled particles with no alignment *Phys. Rev. Lett.* **108** 235702
[16] Redner G S, Hagan M F and Baskaran A 2013 Structure and dynamics of a phase-separating active colloidal fluid *Phys. Rev. Lett.* **110** 055701
[17] Cates M E and Tailleur J 2015 Motility-induced phase separation *Annu. Rev. Condens. Matter Phys.* **6** 219–44
[18] Hasnain J, Menzl G, Jungblut S and Dellago C 2017 Crystallization and flow in active patch systems *Soft Matter* **13** 930–6
[19] Fischer A, Schmid F and Speck T 2020 Quorum-sensing active particles with discontinuous motility *Phys. Rev.* E **101** 012601
[20] Fily Y, Henkes S and Marchetti M C 2014 Freezing and phase separation of self-propelled disks *Soft Matter* **10** 2132–40
[21] Tammo Siebert J, Dittrich F, Schmid F, Binder K, Speck T and Peter V 2018 Critical behavior of active Brownian particles *Phys. Rev.* E **98** 030601
[22] Solon A P, Stenhammar J, Wittkowski R, Kardar M, Kafri Y, Cates M E and Tailleur J 2015 Pressure and phase equilibria in interacting active Brownian spheres *Phys. Rev. Lett.* **114** 198301
[23] Solon A P, Stenhammar J, Cates M E, Kafri Y and Tailleur J 2018 Generalized thermodynamics of motility-induced phase separation: phase equilibria, Laplace pressure, and change of ensembles *New J. Phys.* **20** 075001
[24] Paliwal S, Rodenburg J, van Roij R and Dijkstra M 2018 Chemical potential in active systems: predicting phase equilibrium from bulk equations of state? *New J. Phys.* **20** 015003
[25] Irving J H and Kirkwood J G 1950 The statistical mechanical theory of transport processes: IV. The equations of hydrodynamics *J. Chem. Phys.* **18** 817–29
[26] Yang X, Manning M L and Marchetti M C 2014 Aggregation and segregation of confined active particles *Soft Matter* **10** 6477–84
[27] Fily Y, Kafri Y, Solon A P, Tailleur J and Turner A 2017 Mechanical pressure and momentum conservation in dry active matter *J. Phys. A: Math. Theor.* **51** 044003
[28] Row H and Brady J F 2020 Reverse osmotic effect in active matter *Phys. Rev.* E **101** 062604
[29] Magiera M P and Brendel L 2015 Trapping of interacting propelled colloidal particles in inhomogeneous media *Phys. Rev.* E **92** 012304
[30] Takatori S C and Brady J F 2015 Towards a thermodynamics of active matter *Phys. Rev.* E **91** 032117
[31] Santos A, López de Haro M and Bravo Yuste S 1995 An accurate and simple equation of state for hard disks *J. Chem. Phys.* **103** 4622–5
[32] Bernard E P and Krauth W 2011 Two-step melting in two dimensions: first-order liquid–hexatic transition *Phys. Rev. Lett.* **107** 155704
[33] Tailleur J and Cates M E 2008 Statistical mechanics of interacting run-and-tumble bacteria *Phys. Rev. Lett.* **100** 218103
[34] Elgeti J and Gompper G 2013 Wall accumulation of self-propelled spheres *Europhys. Lett.* **101** 48003
[35] Lee C F 2013 Active particles under confinement: aggregation at the wall and gradient formation inside a channel *New J. Phys.* **15** 055007
[36] Das S, Gompper G and Winkler R G 2019 Local stress and pressure in an inhomogeneous system of spherical active Brownian particles *Sci. Rep.* **9** 6608
[37] Todd B D, Evans D J and Daivis P J 1995 Pressure tensor for inhomogeneous fluids *Phys. Rev.* E **52** 1627–38
[38] Omar A K, Wang Z-G and Brady J F 2020 Microscopic origins of the swim pressure and the anomalous surface tension of active matter *Phys. Rev.* E **101** 012604
[39] Monaghan J J 2005 Smoothed particle hydrodynamics *Rep. Prog. Phys.* **68** 1703–59
[40] Hermann S and Schmidt M 2020 Active interface polarization as a state function *Phys. Rev. Res.* **2** 022003
[41] Patch A, Sussman D M, Yllanes D and Marchetti M C 2018 Curvature-dependent tension and tangential flows at the interface of motility-induced phases *Soft Matter* **14** 7435–45
[42] Fejes L 1940 Über einen geometrischen Satz *Math. Z.* **46** 83–5
[43] Lotito V and Zambelli T 2020 Pattern detection in colloidal assembly: a mosaic of analysis techniques *Adv. Colloid Interface Sci.* **284** 102252